



Transformation of Ag ions to Ag nanoparticles-loaded AgCl microcubes in the plant root zone

Journal:	<i>Environmental Science: Nano</i>
Manuscript ID	EN-ART-01-2019-000088.R1
Article Type:	Paper
Date Submitted by the Author:	01-Mar-2019
Complete List of Authors:	<p>Guo, Huiyuan; University of Massachusetts Amherst, Stockbridge School of Agriculture Ma, Chuanxin; Connecticut Agricultural Experiment Station, Department of Analytical Chemistry Thistle, Lauren ; Stockbridge School of Agriculture, University of Massachusetts, Amherst, MA 01003, USA Huynh, My; Stockbridge School of Agriculture, University of Massachusetts, Amherst, MA 01003, USA Yu, Chenghao; Stockbridge School of Agriculture, University of Massachusetts, Amherst, MA 01003, USA Clasby, Daniel ; Civil and Environmental Engineering, University of Massachusetts, Amherst, MA 01003, USA Chefetz, Benny; Hebrew University of Jerusalem, Soil and Water Sciences Polubesova, Tamara ; Department of Soil and Water Sciences, Hebrew University of Jerusalem, Rehovot 76100, Israel White, Jason; CT Agricultural Experiment Station, Analytical Chemistry He, Lili; Univ. of Massachusetts, Dept. of Food Science Xing, Baoshan; UMASS, Stockbridge School of Agriculture</p>

1 **Environmental Significance Statement**

2 The unique nano effects and wide application of engineered silver nanoparticles have directed
3 huge attention to their release, exposure, behavior and impacts in the environment. However,
4 nanoscale silver particulates are not new in the ecosystem. Naturally formed ones have long been
5 present, but our knowledge on the natural sources of silver nanoparticles and the associated
6 processes is still limited, especially those derived from growing plants. This study, for the first
7 time, demonstrates that the plant root exudate-mediated phototransformation of silver ions to
8 nanosilver can be a natural source of silver nanoparticles in the plant root zone, which broadens
9 our understanding on the environmental behavior and fate of silver ions and their transformed
10 products. We also quantitatively analyzed the silver speciation during the transformation of
11 silver ions in the plant root zone and investigated the mechanisms underlying the bio-induced
12 formation of silver nanoparticles, which provides a valuable knowledge base for future
13 evaluation of their impacts on environmental health and agricultural safety.

1
2
3 **Transformation of Ag ions to Ag nanoparticles-loaded AgCl microcubes in the plant root zone**
4

5
6 *Huiyuan Guo,[†] Chuanxin Ma,[§] Lauren Thistle,[†] My Huynh,[†] Chenghao Yu,[†] Daniel Clasby,[#]*
7
8 *Benny Chefetz,^{||} Tamara Polubesova,^{||} Jason C. White,[§] Lili He,^{‡,*} Baoshan Xing^{‡,*}*
9

10
11 [†] Stockbridge School of Agriculture, University of Massachusetts, Amherst, MA 01003, USA
12

13
14 [‡] Department of Food Science, University of Massachusetts, Amherst, MA 01003, USA
15

16
17 [§] Department of Analytical Chemistry, The Connecticut Agricultural Experiment Station, New
18
19 Haven, CT 06511, USA
20

21
22 [#] Civil and Environmental Engineering, University of Massachusetts, Amherst, MA 01003, USA
23

24
25 ^{||} Department of Soil and Water Sciences, Hebrew University of Jerusalem, Rehovot 76100,
26
27 Israel
28

29
30
31
32 *Corresponding Authors
33

34
35 Dr. Baoshan Xing, Tel.: +1 413 545 5212; E-mail: bx@umass.edu
36

37
38 Dr. Lili He, Tel.: +1 413 545 5847; E-mail: lilihe@foodsci.umass.edu
39
40
41
42
43
44
45
46
47
48
49
50
51
52
53
54
55
56
57
58
59
60

Abstract

Natural formation of metal nanoparticles is an important pathway that will modify the fate, behavior, and biological availability of heavy metal ions in the environment. Most work has focused on the ability of natural organic matter (NOM) and extracellular polymeric substances (EPS) to convert metal ions to nanoparticles. However, plant roots, ubiquitous in soil and aquatic environments, may have a significant role in the formation of naturally occurring metal nanoparticles. This work demonstrates the importance of plant roots and associated exudates in mediating the transformation of Ag^+ in the presence of sunlight. Using Ag^+ as the starting material, transformation took place in three steps: 1) formation of AgCl microcubes (μAgCl) through complexation of Ag^+ by plant-released chloride ions in root exudates; 2) stabilization of μAgCl by biomolecules in root exudates; and 3) partial photoreduction of μAgCl to $\text{Ag}(0)$ nanoparticles (nAg) facilitated by exudate biomolecules. Morphological and compositional changes were observed by scanning electron microscopy with energy dispersive X-ray spectroscopy (SEM-EDS) on the particles from 0-24 h: Cubic AgCl microcrystals were converted to cauliflower-shaped core-shell structures with nAg clusters as the shell and μAgCl as the core. The quantification of Ag^+ , μAgCl and nAg species over time demonstrates that the transformation kinetics fit ($R^2=0.99$) a second-order reaction ($k=1.11 \text{ mM}^{-1} \cdot \text{h}^{-1}$). The discovery of plant root exudate-mediated phototransformation of Ag^+ adds new knowledge to our understanding of Ag transformation in plant root zone and will guide the assessment of both exposure and risk in the environment.

Introduction

Human use of silver metal can be traced back 7000 years.¹ Its corrosion tolerance and antimicrobial activity have led to wide application in coins, silverware, jewelry and medical devices. When silver metal is in contact with water, body fluid or tissue exudates, dissolution can occur with silver ions (Ag^+) being released and yielding antimicrobial activity.² With the rapid development of nanotechnology, the uniqueness of silver has been broadened at the nanoscale. Silver nanoparticles (nAg) have enhanced physicochemical and biological properties, including increased antimicrobial activity, largely due to the large specific surface area for ion release. Applications of nAg have been known for more than 100 years. The particles are broadly used in a variety of fields, including photography, biomedical devices/treatments, food processing, and agricultural products.^{1,3,4} Given the numerous applications of nAg, concerns over their potential toxicity and environmental impacts have arisen. Many studies have suggested that the toxicity of nAg was mainly attributed to released Ag^+ .^{5,6} For example, nAg can be readily oxidized to form a surface layer of Ag_2O (solubility product equilibrium constant, $K_{\text{sp}}=4\times 10^{-11}$), which further dissolves in water as Ag^+ and subsequently increases the toxicity.⁷

Regardless of the particle size, silver metal or nAg can release Ag^+ into aquatic systems, sediments, or soils. In addition to potential release from silver metal and nAg, Ag^+ may also be discharged directly from Ag^+ -containing sources such as disinfection products, photographic films and silver stains. Ag^+ is both chemically and biologically reactive, and understanding of its transformation in natural environments is important to appropriately assess risk. The reduction of Ag^+ to nAg by natural organic matter⁸⁻¹¹ or microorganism exudates (i.e., extracellular polymeric substances)^{12,13} through electron transfer has been widely reported. However, Ag^+ transformation in the plant root zone prior to root uptake is poorly understood. Gardea-Torresdey

1
2
3 et al. first reported the formation of nAg by a living plant system.¹⁴ Their study on alfalfa sprouts
4 showed that Ag^+ (0, 40, 80, 160, and 320 mg/L) in agar solidified nutrient media could be
5 reduced to $\text{Ag}(0)$, which was further absorbed by roots and transferred to shoots. They suggested
6 the coalescence of $\text{Ag}(0)$ atoms could be a self-protective response of plants. However, the
7 authors did not mention the substances responsible for the reduction of Ag^+ to $\text{Ag}(0)$ in agar
8 media. Pardha-Saradhi et al. observed that roots of intact plants of 16 species from 11 diverse
9 families of angiosperms caused the exogenous formation of nAg when incubated in AgNO_3
10 solutions (0.05 mM-2 mM) for 6-12 h.¹⁵ The proposed mechanism involved the inherent
11 reducing potential from root plasma membrane-bound dehydrogenases; the authors reported that
12 root exudates did not contribute to the formation of nAg. There are also several publications that
13 used live plants or plant tissue extracts as a “green” synthesis approach to produce nAg.¹⁶⁻²⁰
14 However, in these studies, the formation mechanisms, kinetics and morphology of plant-derived
15 nAg, as well as potential environmental impacts of the transformation, are not well defined. A
16 previous study evaluating the antibacterial activities of nAg and Ag^+ showed that the
17 nanoparticles were less toxic than Ag^+ , especially under anaerobic conditions, because the
18 effective concentration of nAg to bring about an antibacterial effect on 50% of the test bacteria
19 (*Escherichia coli*) was much lower than that of Ag^+ ($[\text{nAg}]_{\text{EC50}} = 2.04 \pm 0.07 \text{ mg/L}$ vs $[\text{Ag}^+]_{\text{EC50}} =$
20 $0.10 \pm 0.01 \text{ mg/L}$).⁵ Similar findings were also reported by others.^{1,6,21,22} Importantly, the
21 exogenous generation of plant root-derived nAg from Ag^+ may significantly modify the risk
22 associated with Ag^+ released into the environment. As such, the goal of this study is to unravel
23 the mechanism and factors that control the transformation of Ag^+ to nAg in plant root zone. We
24 propose that root exudates, a mixture of organic molecules and inorganic ions, play an important
25 role in this process. To test this idea, we not only examined the function of organic molecules,
26
27
28
29
30
31
32
33
34
35
36
37
38
39
40
41
42
43
44
45
46
47
48
49
50
51
52
53
54
55
56
57
58
59
60

1
2
3 but also inorganic ions in root exudates, such as Cl^- . Previous studies have shown that electrons
4 excited from the valance band to the conduction band of AgCl(s) under light irradiation can
5 result in the formation of nAg due to the reduction of Ag^+ .^{23–25} It is of importance to figure out if
6 Cl^- can modify the transformation of Ag^+ to nAg through the formation of AgCl , given the
7 ubiquitous existence of Cl^- in root exudates.
8
9

10 In this work, we discover sunlight irradiation and root exudates are the key factors controlling
11 the Ag^+ transformation to nAg -containing particles in plant root zone. Moreover, transformation
12 products over time were characterized and quantified to demonstrate the kinetics and mechanism.
13
14 This study provides new perspective on the transformation, speciation, stability and potential
15 toxicity of Ag^+ in biological systems.
16
17
18
19
20
21
22
23
24
25
26

27 **Experimental section**

28 **Materials**

29
30
31 Triton™ X-114, sodium thiosulfate, nitric acid (70%) and ferbam were purchased from Fisher
32 Scientific (Pittsburgh, PA). Silver nitrate (ACS reagent, $\geq 99.0\%$), polyvinylpyrrolidone (PVP),
33 ethylenediaminetetraacetic acid (EDTA) and diphenyleneiodonium (DPI) were obtained from
34 Sigma-Aldrich (St. Louis, MO). Wheat seeds were acquired from Johnny's Selected Seeds. All
35 reagent solutions were prepared using Milli-Q water ($18 \text{ M}\Omega \cdot \text{cm}$) unless indicated otherwise.
36
37
38
39
40
41
42
43
44
45

46 **Methods**

47 **Transformation experiments**

48
49 Transformation experiments were conducted in a greenhouse ($25 \text{ }^\circ\text{C}$ with 16 h/8 h (light/dark)
50 cycle, light intensity $\sim 600 \text{ }\mu\text{mol m}^{-2} \text{ s}^{-1}$) with wheat plants (*Triticum aestivum*). The wheat plants
51
52
53
54
55
56
57
58
59
60

1
2
3 were germinated and grown in moisturized vermiculite for one week. To evaluate the reducing
4 ability of wheat seedlings, roots of intact plants were gently washed by nanopure water and
5 incubated with AgNO_3 (1 mM, 8 mL, and pH ~5.6). Incubation vials were completely or partially
6 wrapped with aluminum foil to evaluate the light effect on Ag^+ transformation. All the Ag^+
7 transformation experiments were performed in triplicate. Three wheat seedlings were used in
8 each replicate. After having a good understanding of the Ag^+ transformation process and
9 mechanism by wheat plants, we extended our investigation to an aquatic plant, *Lolium*
10 *multiflorum*,^{26,27} using similar settings except with lower Ag^+ concentrations (0.05-0.5 mM).
11
12
13
14
15
16
17
18
19
20
21

22 **The functions of wheat root plasma membrane-bound enzymes or root exudates**

23
24
25 The mechanism of light-induced transformation in the root zone was examined by focusing on
26 two possible pathways; root plasma membrane-bound enzymes or root exudates. Crude root
27 enzymes were extracted through centrifugation (13,500 rpm at 4 °C) after homogenizing wheat
28 roots in 50 mM phosphate buffer (pH 7.1) with 5% PVP and 5 mM EDTA.¹⁵ The isolated root
29 enzymes were incubated with Ag^+ with light irradiation. Enzyme-deactivated controls were
30 obtained by boiling isolated exudates prior to Ag^+ exposure. DPI was used as a dehydrogenase
31 inhibitor to evaluate the role of plasma membrane-bound dehydrogenases.²⁸ Furthermore, the
32 function of root exudates was tested after removing the plant roots from the Ag^+ incubation
33 solution, and the remaining Ag species and root exudates (pH ~5.6) were examined over the
34 course of 24 h in the presence of light. To estimate the concentration of root exudates in the
35 system, a total carbon analyzer (Shimadzu, TOC-L) was used to measure the total organic carbon
36 (TOC) and inorganic carbon. According to the analysis, the TOC was 228.88 ± 12.44 mg/L and
37 inorganic carbon was 1.02 ± 0.05 mg/L.
38
39
40
41
42
43
44
45
46
47
48
49
50
51
52
53
54
55
56
57
58
59
60

Characterization of the Ag⁺ transformation products

Multiple techniques were used to characterize the Ag⁺ transformation products. UV-Vis spectroscopy (Agilent 8453) was used to measure the absorbance of the reaction solutions and monitor Ag⁺ transformation. At a given time, freshly prepared samples were vortexed for 10 seconds and then analyzed by UV-Vis spectroscopy immediately. Hydrodynamic diameter of the formed particles was determined by dynamic light scattering (DLS, Brookhaven, 90Plus); particle X-ray powder diffraction (XRD) patterns were acquired by a PANalytical X'Pert diffractometer using Cu K α radiation. Scanning electron microscopy (SEM, FEI Magellan 400 XHR) with energy dispersive X-ray spectroscopy (EDS, Oxford 80 mm² X-Max) was used to investigate the morphology, structure and speciation of the formed nanoparticles. The sample preparation for SEM-EDS can be found in the SI (Section 1).

Surface chemistry of the formed particles was characterized by Raman spectroscopy and Fourier-transform infrared spectroscopy (FTIR). In addition, the formation of nAg in the samples was confirmed by using a surface-enhanced Raman spectroscopy (SERS)-based method previously established in our group²⁹ with minor revision. The approach used ferbam as an indicator molecule; the enhanced signals of the indicator-nAg complex were readily detectable by SERS.²⁹ The experimental procedure and settings for all three methods were detailed in the SI (Section 2).

Measurement of the transformation of Ag⁺ to μ AgCl and nAg

In the samples thought to contain a mixture of Ag⁺/ μ AgCl/nAg, the separation of Ag species were performed through a selective centrifugation-dissolution-centrifugation method by Yin et al.³⁰ with minor revisions. The separation of the formed particles from Ag⁺ was achieved by high-speed centrifugation (13,500 rpm) in Eppendorf tubes (1.5 mL) for 30 min. The supernatant containing Ag⁺ was collected as S1 while the particle pellets were re-suspended in 0.1% (w/v)

1
2
3 Triton X-114 and 20 mM $\text{Na}_2\text{S}_2\text{O}_3$ for the second cycle of centrifugation and isolation. Here, 0.1%
4
5 (w/v) Triton X-114 was used as a coating agent to protect the stability of nAg. Meanwhile,
6
7 μAgCl were dissolved by incubating with 20 mM $\text{Na}_2\text{S}_2\text{O}_3$ for 5 min. $\text{Na}_2\text{S}_2\text{O}_3$ could enable the
8
9 separation of μAgCl from nAg because of the high ability of thiosulfate to replace Cl in AgCl
10
11 and form soluble silver complexes. The solution was further centrifuged at 13,500 rpm for 30
12
13 min to separate nAg from the newly dissolved silver (originally from μAgCl). The supernatant
14
15 was collected as S2 to represent Ag content in μAgCl . The precipitates (P), which contained nAg,
16
17 were digested by concentrated HNO_3 (0.5 mL) and diluted using water to ensure less than 3%
18
19 HNO_3 prior to analysis. S1 and S2 were digested in a similar way. Ag content in S1, S2 and P
20
21 was measured by inductively coupled plasma-mass spectrometry (ICP-MS 2030, Shimadzu) and
22
23 the total Ag content in a given sample was calculated as $\text{S1}+\text{S2}+\text{P}$. To confirm the accuracy of
24
25 using $\text{S1}+\text{S2}+\text{P}$ to estimate total Ag, we directly measured the total Ag in the sample of 24-h
26
27 light exposure by ICP-MS, which is 0.42 ± 0.05 mM, highly close to $\text{S1}+\text{S2}+\text{P}$ (0.41 ± 0.004
28
29 mM) in the same sample. Furthermore, we found the total amount of Ag based on the calculation
30
31 of $\text{S1}+\text{S2}+\text{P}$ was consistently ~ 0.4 mM over 0-24 h of light exposure (Figure 3c). The well-
32
33 maintained mass balance demonstrated the reliability of ICP-MS measurements at different time
34
35 points and the accuracy of using $\text{S1}+\text{S2}+\text{P}$ to estimate total Ag. Moreover, our evaluation of
36
37 accuracy on amended control samples was $106.5 \pm 2.9\%$ for AgCl (0.33 mM) and $89.8 \pm 3.5\%$ for
38
39 nAg (60 nm, citrate, 10 mg/L). In addition, ion chromatography (Metrohm 850 Professional IC)
40
41 was used to measure the Cl^- in S1 and S2, which represents free Cl^- in the solution and chloride in
42
43 μAgCl . The reliability of the Cl^- measurement was tested with two Cl^- standards (0.14 mM and
44
45 0.7 mM) and the recovery rates were $90.5 \pm 0.7\%$ and $96.1 \pm 3.1\%$, respectively.
46
47
48
49
50
51
52
53

54 **Test on the reduction of Ag^+ by organic molecules in root exudates**

55
56
57
58
59
60

1
2
3 In order to test the reduction of Ag^+ by organic molecules in root exudates independently, the
4 interference by the photoreduction of AgCl was excluded by removing Cl^- in root exudates
5 before interaction with Ag^+ . The removal of Cl^- was achieved through adding Ag^+ to form AgCl
6 microparticles that could be removed through 100 kDa ultra-centrifugal filter membranes
7 (Amicon Ultra-15, Millipore). The pore size of the membrane is about 3 nm, which can ensure
8 that most organic molecules in root exudates can pass through while microscale AgCl was
9 trapped on the membrane and removed from the root exudates. The removal of AgCl was
10 confirmed complete based on that the UV-Vis absorbance peak of AgCl did not show up after
11 adding Ag^+ into the filtrate. In the group without Cl^- removal, we added the same amount of Ag^+ .
12 The reduction of Ag^+ by root exudates with/out Cl^- removal was recorded and compared over 24
13 h.
14
15
16
17
18
19
20
21
22
23
24
25
26
27
28
29

30 **Results and Discussion**

31 **Light effect**

32
33 To demonstrate how light impacted Ag^+ transformation, comparative experiments were
34 conducted under light and dark conditions. As shown in Figure 1a, an obvious color difference
35 was observed, with the light-exposed (L) solution in dark brown while the sample without light
36 (NL) was somewhat cloudy white. It is noted that before transformation, the solution color was
37 transparent and colorless (Figure 1b). UV-Vis spectrum of the L solution showed two absorbance
38 peaks at 385 and 560 nm; the NL solution did not have these peaks (Figure 1b). The 385 nm
39 peak is representative of the surface plasmon resonance of nAg, suggesting light-induced
40 nanoparticle formation. The secondary peak at 560 nm may derive from aggregated nAg^{9,31} or
41 composites of nAg with other particulate Ag species³². These findings indicate that light is likely
42
43
44
45
46
47
48
49
50
51
52
53
54
55
56
57
58
59
60

critical for the transformation of Ag^+ to nAg-containing particles in wheat root zone. Previous studies also demonstrated the generation of exogenous nAg in plant root system.^{14,15} However, it is unclear whether light played a role or not in the transformation since it was not mentioned. It appears that our study is the first to report the light-induced formation of nAg-containing particles in the root zone of live plants.

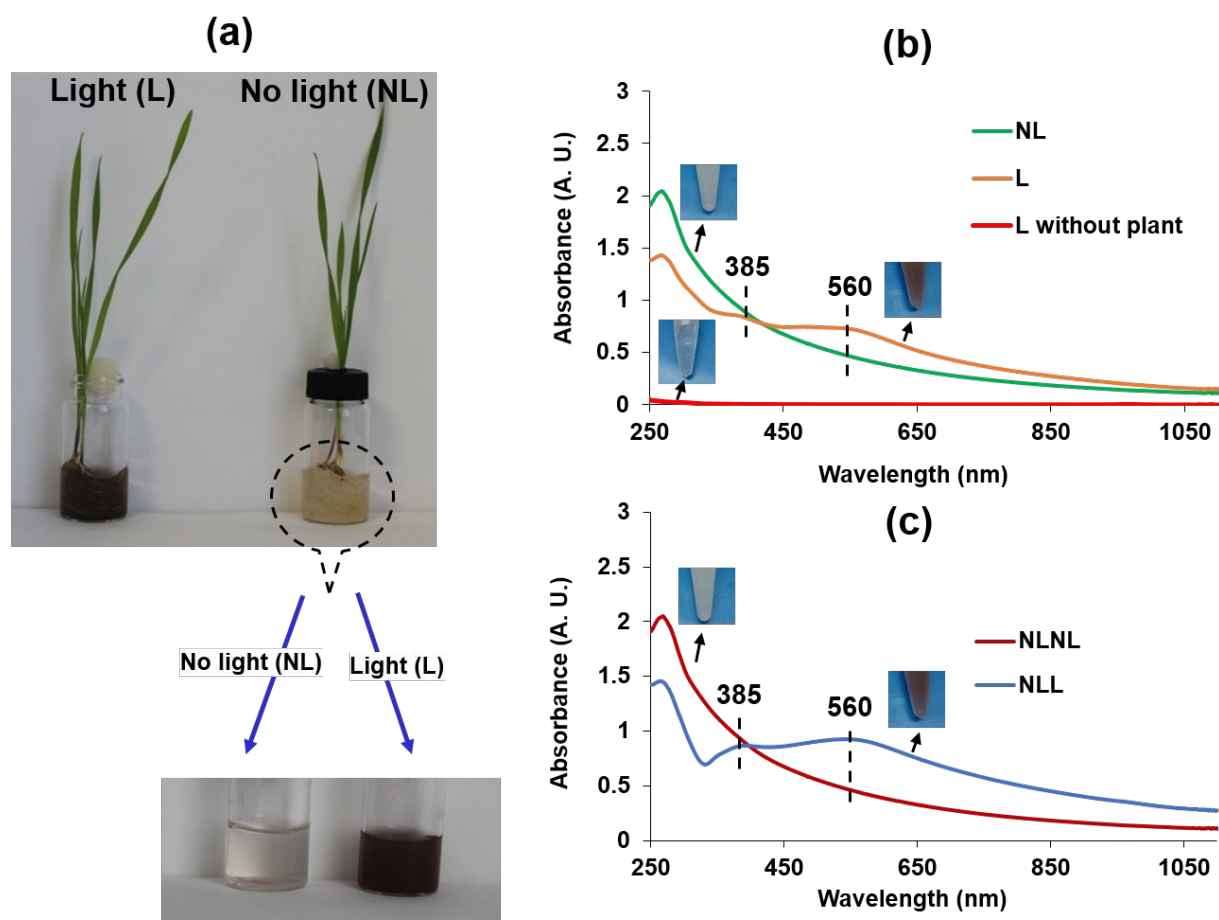


Figure 1. Light is a critical factor controlling the reduction of Ag^+ to nAg in the plant root zone.

(a) Comparison of the color change of Ag^+ solution (1 mM) with (L) and without light exposure (NL) after incubation with live roots of intact plants for 24 h. (b) UV-Vis spectra of the growth solutions from (a) and a control (Ag^+ , 1 mM) without plants. (c) UV-Vis spectra of the growth solution (NL) from (a) with further light (NLL) or no light exposure (NLNL) (24 h) after

1
2
3 removing plant roots. The similar UV-Vis pattern between L and NLL indicates that root
4
5 exudates in the growth solution contributed to the light-induced reduction of Ag^+ .
6
7
8
9

11 **Transformation mediator**

12
13
14 It is apparent that sunlight can provide energy to drive the reduction reaction, but which pathway
15
16 leads to the electron transfer is not well understood. There are two possible mediators of the nAg
17
18 generation: root plasma membrane-bound dehydrogenases and root exudates. The rationale for
19
20 the selection is based on that root plasma membrane-bound dehydrogenases have reductase
21
22 activity, and meanwhile, the root exudates, as a cocktail of both inorganic ions and organic
23
24 biomolecules, may induce the transformation of Ag^+ .
25
26

27
28 To evaluate the role of root plasma membrane-bound dehydrogenases, DPI was used as an
29
30 inhibitor to specifically deactivate dehydrogenase in the isolated root enzymes.²⁸ After
31
32 incubation with Ag^+ in the presence of light, the potential formation of nAg was compared
33
34 between the groups with/out DPI addition (Figure S1). As shown in Figure S1a, the group with
35
36 DPI showed a similar absorbance pattern as the control (without DPI), indicating that the
37
38 inhibition of root plasma membrane-bound dehydrogenases did not affect the reduction of Ag^+ .
39
40 The apparent lack of correlation of color change with root enzymes was further confirmed by a
41
42 comparison between raw root enzymes and boiled root enzymes (Figure S1b). Although boiling
43
44 would deactivate root enzymes,⁹ this heating did not inhibit the formation of nAg. Taken
45
46 together, root enzymes including plasma membrane-bound dehydrogenases were not responsible
47
48 for the exogenous formation of nAg in a live plant root system. The reason that the isolated crude
49
50 root enzyme extract led to the reduction of nAg here and in a previous study¹⁵ is most likely due
51
52 to other biomolecules in root tissues unrelated to root plasma membrane-bound enzymes. For
53
54
55
56
57
58
59
60

1
2
3 example, it has been reported that reducing sugars^{33,34} and flavonoids^{35,36} rich in plant tissue
4
5 extracts can act as reducing agents for nAg. However, in this study, we found that nAg was
6
7 formed outside of live plant roots. These biomolecules buried inside the root cells are not likely
8
9 to be a contributor of the exogenous generation of nAg in the plant root zone.
10
11

12
13 To independently examine the function of root exudates in transforming Ag^+ , we isolated root
14
15 exudates from live plant roots in the presence of Ag^+ under dark condition (NL). After 24 h, the
16
17 intact plant roots were removed from the container. At this point, the solution contained a
18
19 mixture of Ag^+ and root exudates, and the color was cloudy white. We divided the solution into
20
21 two portions; one portion was exposed to sunlight (NLL) while the other was fully covered by
22
23 aluminum foil to prevent light exposure (NLNL). After another 24 h, the UV-Vis spectra of the
24
25 two portions were measured (Figure 1c). The group with light irradiation demonstrated two
26
27 characteristic peaks (385 nm and 560 nm) similar to those formed by live plant roots under light
28
29 exposure; the samples without light exposure remained cloudy white. The similarity in both color
30
31 change and UV-Vis absorbance between live root-induced and root exudate-induced Ag^+
32
33 transformations confirms that the formation of nAg-containing particles is due to components in
34
35 the exudates. Pardha-Saradhi et al. reported that root exudates did not contribute to nAg
36
37 formation because the medium where the plant roots had been incubated for 24 h did not yield
38
39 particles.¹⁵ Importantly, the role of light in inducing the nAg generation was not considered. As
40
41 evident in the current study, the formation of nAg in a live plant root system is light-driven and
42
43 root exudate-mediated; not accounting for the complexity of this reaction likely explains the
44
45 discrepancy between the two studies.
46
47
48
49
50
51
52
53
54
55
56
57
58
59
60

Composition of the formed particles

The difference in the UV-Vis spectrum pattern shown in Figure 1b demonstrates the transformation and composition change induced by light irradiation. Without light exposure, the sample had an absorbance peak at ~ 270 nm, which is actually a typical signal of AgCl.^{37–39} However, with light exposure, the UV-Vis spectrum pattern of the solution showed a decrease in the peak absorbance at ~ 270 nm while two nAg-related peaks at 385 nm and 560 nm became evident, indicating light-induced transformation of AgCl to nAg. The presence of AgCl in the non-irradiated controls and the co-presence of nAg and AgCl in the light-exposed samples (Figure 1b) was further verified by XRD analysis (Figure 2a). As expected, the samples without sunlight showed a clear XRD pattern for AgCl.^{40,41} Upon light exposure, a diffraction peak of metallic Ag occurred at around 38° in the XRD spectrum, confirming the transformation of AgCl to Ag(0).^{40,41}

In order to remove the interference of AgCl on the characterization of nAg, $\text{Na}_2\text{S}_2\text{O}_3$ was used to dissolve AgCl in the composite samples. After AgCl removal, the solution color changed from dark brown to light brown, signifying shifts in composition and particle size. To characterize the likely changes, we measured the UV-Vis absorbance and particle size before and after AgCl removal (Figure 2b). Before removal, the nAg/AgCl mixture had three peaks: 270, 385 and 560 nm. With removal, only the nAg peak remained; this was accompanied by a red shift from 385 nm to 410 nm, likely caused by the structural change resulting from AgCl dissolution. The disappearance of the peak at ~ 560 nm implies that this signal originated from nAg/AgCl composite and the subsequent dissolution of AgCl degraded the composite. Kracht et al.³² similarly reported that a peak at 550–580 nm was derived from nAg/AgCl composites. We also noted that after AgCl removal the peak at ~ 270 nm (Figure 2b, 3b and S3) came from the

protecting agent TX-114 as demonstrated in a control sample with TX-114 alone (Figure S2). In addition to the compositional change, the hydrodynamic diameter of particles in the solution decreased from 219.6 ± 13.4 nm to 93.8 ± 5.3 nm after AgCl removal. Based on the color change and characterization of the transformed products, the observed dark brown color was derived from the nAg/ μ AgCl composites. With the dissolution of μ AgCl, only nAg was present in the solution, which changed the solution color to light brown.

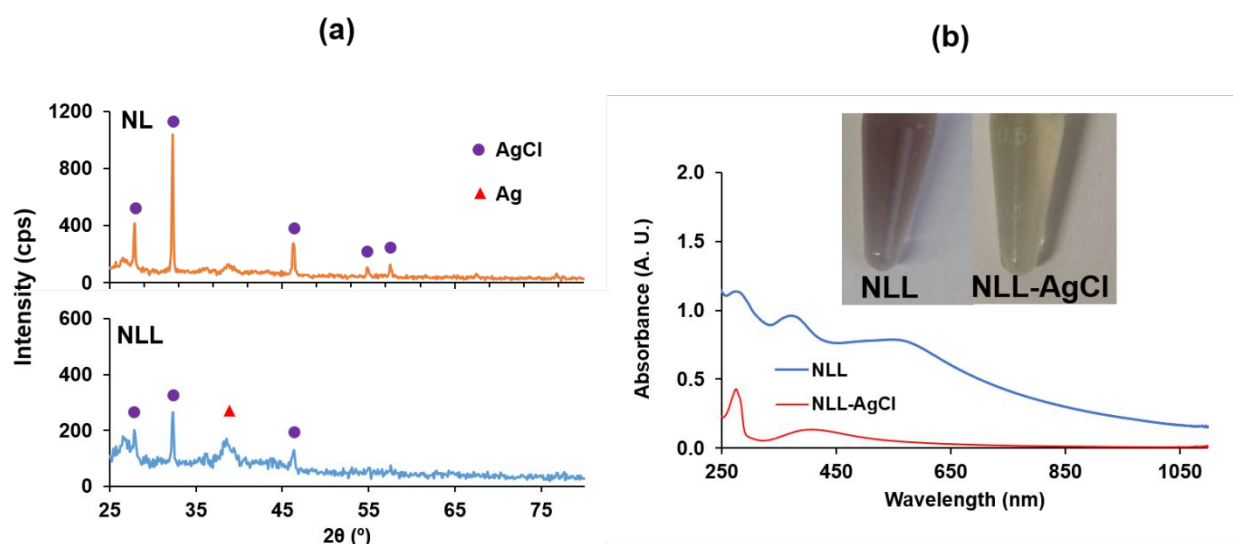


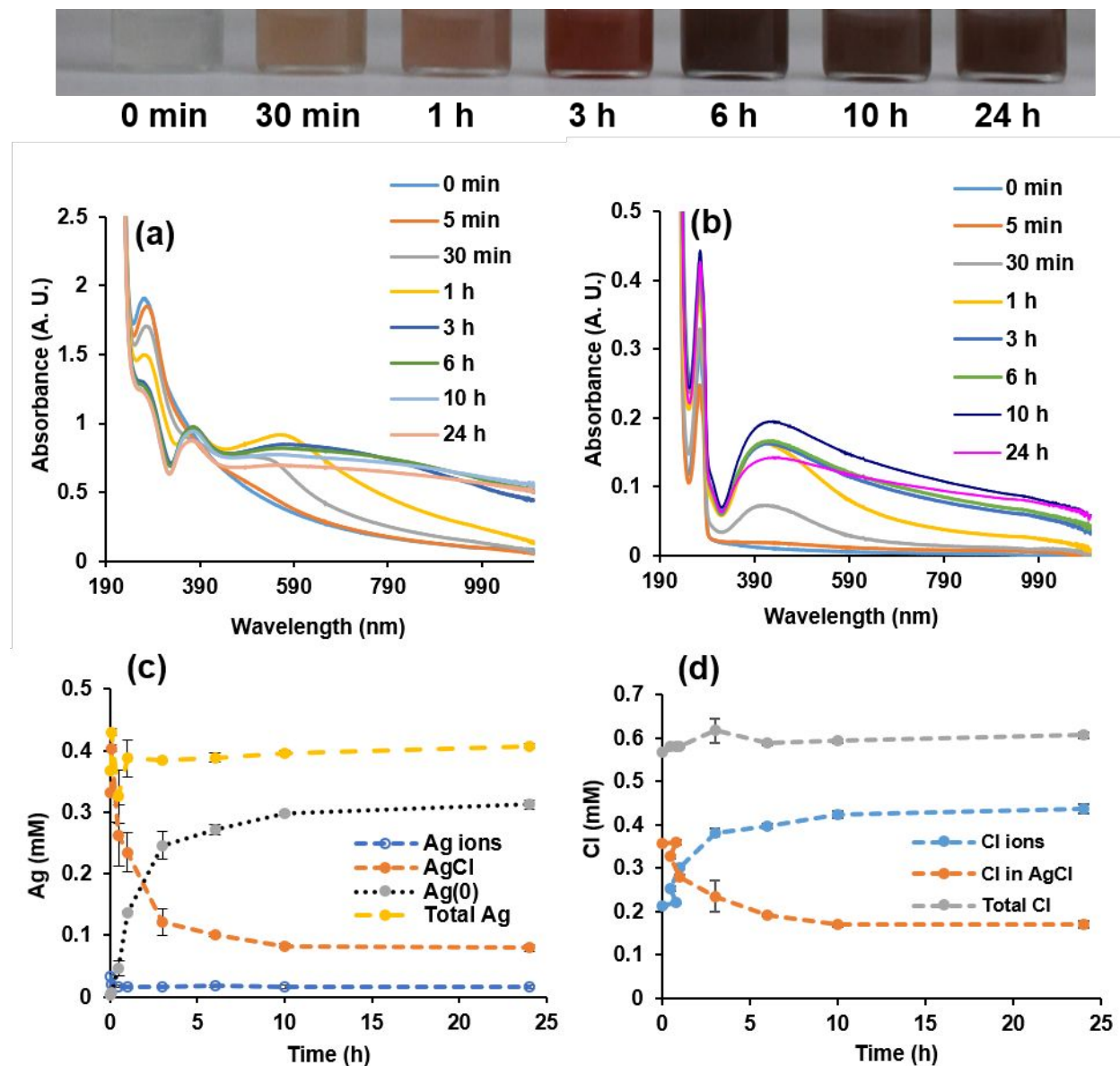
Figure 2. (a) XRD analysis of the formed particles before (NL) and after light exposure (NLL). (b) UV-Vis absorbance of the formed particles before (NLL) and after removal of AgCl (NLL-AgCl) (Inset: the solution colors of the formed particles).

Transformation dynamics and fractionation of silver species

After demonstrating that root exudates mediate the sunlight-induced transformation of Ag^+ to nAg/ μ AgCl, we sought to elucidate the dynamics of this process. As shown in Figure 3, the solution color gradually changed from white to orange to reddish brown then to dark brown over the course of 10 h. The color then seemed to stabilize from 10 h to 24 h. The UV-Vis absorbance

1
2
3 of these samples was measured at the same time points (Figure 3a). At the outset, there was only
4 one peak at ~270 nm. As irradiation began, this peak shifted to 280 nm. As mentioned above, the
5 peak at 270-280 nm is representative of μAgCl . The slight red shift probably indicates the
6 morphology change upon light irradiation. Subsequently, the intensity of this peak decreased
7 while two new peaks appeared at 385 nm and 550 nm. The typical peak of $\text{nAg}/\mu\text{AgCl}$ at 550 nm
8 exhibited increased intensity and a red shift to 580 nm as the reaction proceeded from 0 h to 1 h.
9 The intensity subsequently decreased from 1 h to 24 h. Meanwhile, the peak at 385 nm, which is
10 attributed to nAg , increased from 0 min to 3 h and then slightly decreased afterwards. This
11 decrease was likely caused by aggregation as indicated by the zeta potential change of the
12 formed particles over time (Figure S4). Specifically, a zeta potential increase (-24.57 ± 0.11 to -
13 18.00 ± 0.38 mV) occurred from 3 h to 24 h. Another possibility is that the particle size increase
14 from 3 h to 24 h as noted in the SEM data (Figure 4) may have facilitated precipitation. Based on
15 the changes of solution color and the UV-Vis absorbance data, the transformation dynamics
16 seem to occur as follows: 1) initial formation of μAgCl upon Ag^+ contact with root exudates as
17 indicated by the cloudy white appearance and UV-vis absorbance at ~270 nm; 2) partial
18 transformation of μAgCl to nAg upon light irradiation as shown by a decrease of the AgCl peak
19 (270-280 nm), and the appearance of a $\text{Ag}(0)$ peak at 385 nm, as well as a third peak at ~550-580
20 nm representing the $\text{nAg}/\mu\text{AgCl}$ composites. To separately demonstrate the formation dynamics
21 of nAg , the UV-Vis spectra of all samples were analyzed after removal of μAgCl (Figure 3b). As
22 expected, a UV-Vis peak was shown at 410 nm, which is within the typical absorbance range of
23 nAg . The peak increased from 0-10 h and decreased at 24 h. The increase indicates a continuous
24 transformation of μAgCl to nAg from 0-10 h; the decrease at 24 h might be caused by nAg
25 aggregation. As noted above, the surface charge decrease and particle size increase (Figure 4)

likely contributed to nAg aggregation. The increasing formation of nAg from 0 to 10 h was further confirmed by SERS (Figure S7). The rationale and theory of this technique for



nanoparticle detection were demonstrated in our previously published studies.^{29,42,43} The increased signals of ferbam proved the gradual reduction of μAgCl to nAg over the course of 10 h.

Figure 3. Light-induced formation of nAg/ μAgCl over time (0-24 h). UV-Vis absorbance of the formed particles before (a) and after (b) removal of AgCl. Inset in panel (a): enlarged absorbance

1
2
3 peak at 385 nm. The Ag concentration in different fractions (Ag^+ , μAgCl and nAg) at different
4
5 time points (c) were determined by ICP-MS. Meanwhile, the content of chloride as free chloride
6
7 ions in solution and as insoluble chloride in μAgCl at different time intervals (d) were quantified
8
9
10 by IC.

11
12
13
14
15
16 To quantitatively determine the fractionation of silver species over a time series, we utilized ICP-
17
18 MS to quantify the Ag speciation of Ag^+ , μAgCl , and nAg . As shown in Figure 3c, the total
19
20 amount of Ag in the root exudate solution after removing plant roots was about 0.4 mM. The
21
22 lower concentration of Ag than the originally added Ag (1 mM) is because a portion of Ag had
23
24 been adsorbed or absorbed by plant roots during the root exudate collection. The remaining Ag
25
26 stayed at a stable level over the light-induced transformation. At the initial stage, most Ag was
27
28 present as AgCl (>90%) because the released Cl^- had higher concentration than Ag^+ . As the
29
30 transformation proceeded, the fraction of μAgCl decreased from 0 h to 10 h and stabilized at
31
32 ~ 0.1 mM from 10 h to 24 h, which is in a good agreement with the UV-Vis absorbance data. At
33
34 24 h, 80% of the μAgCl was transformed to nAg ; the nAg amount from 0-24 h increased from 0
35
36 mM to ~ 0.3 mM. In addition to monitoring the time-dependent transformation of Ag species, we
37
38 also analyzed the change in chloride as soluble ions or as insoluble μAgCl over time (Figure 3d).
39
40
41 The IC data showed that at 0 min, the total content of chloride (0.57 ± 0.001 mM) was higher than
42
43 that of Ag (0.37 ± 0.01 mM), which agrees with μAgCl instead of Ag^+ being the primary silver
44
45 species in the beginning. The concentration of free Cl^- in the solution increased as μAgCl was
46
47 transformed to nAg and free Cl^- . At 10 h, the chloride level in μAgCl reached equilibrium at 0.17
48
49 mM, which is one-fold higher than the equilibrium concentration of Ag (0.079 mM) in μAgCl . It
50
51 is possible that there were other Ag species, such as AgCl_2^- and AgCl_3^{2-} , attached to the surface
52
53
54
55
56
57
58
59
60

1
2
3 of μAgCl and the newly formed nAg .^{44,45} When the ratio of ionic Cl/Ag in the solution is low,
4 most chloride is present as AgCl . However, in this study as more Cl^- was released into the
5 solution during the reduction of μAgCl , the ratio of ionic Cl/Ag locally increased around the
6 particle surface; AgCl_x^{1-x} could form on the surface of AgCl and even on the nAg .^{44,45}
7
8
9
10
11
12

13 **Structure, morphology and surface chemistry**

14
15

16 Although the composition of the formed particles was defined and quantified above, their
17 structure, morphology and surface chemistry are still unknown; this knowledge is critical for
18 understanding how μAgCl was associated with nAg and what molecules defined the surface
19 chemistry. As such, we first used SEM to characterize the size and morphology of the formed
20 particles (Figure 4). The images showed that before irradiation, cubic μAgCl with an average
21 diameter of about 120 nm were present in the mixture of root exudates and Ag^+ . Upon irradiation,
22 smaller spherical nanoparticles were formed on the surface of cubic μAgCl . Interestingly, the
23 spherical nanoparticles seemed to increase in size as the light exposure extended. At 3 h,
24 nanoparticles with a mean diameter of 32.2 ± 0.6 nm were evident on the surface of μAgCl
25 (154.6 ± 2.3 nm). At 24 h, the transformed particles were of a cauliflower shape with an overall
26 diameter of 207.5 ± 2.8 nm and 40.4 ± 1.3 nm spherical particles on the surface. The morphology
27 change from cube to cauliflower led to a near doubling in whole particle size (120.2 ± 1.8 nm to
28 207.5 ± 2.8 nm). Moreover, during the course of the reaction, smaller $\text{nAg}/\mu\text{AgCl}$ disappeared and
29 bulky aggregates of $\text{nAg}/\mu\text{AgCl}$ were formed; this can be explained by Ostwald ripening, a
30 phenomenon whereby smaller particles of higher surface energy tend to deposit onto larger
31 particles of lower surface energy.^{46,47}
32
33
34
35
36
37
38
39
40
41
42
43
44
45
46
47
48
49
50
51
52
53
54
55
56
57
58
59
60

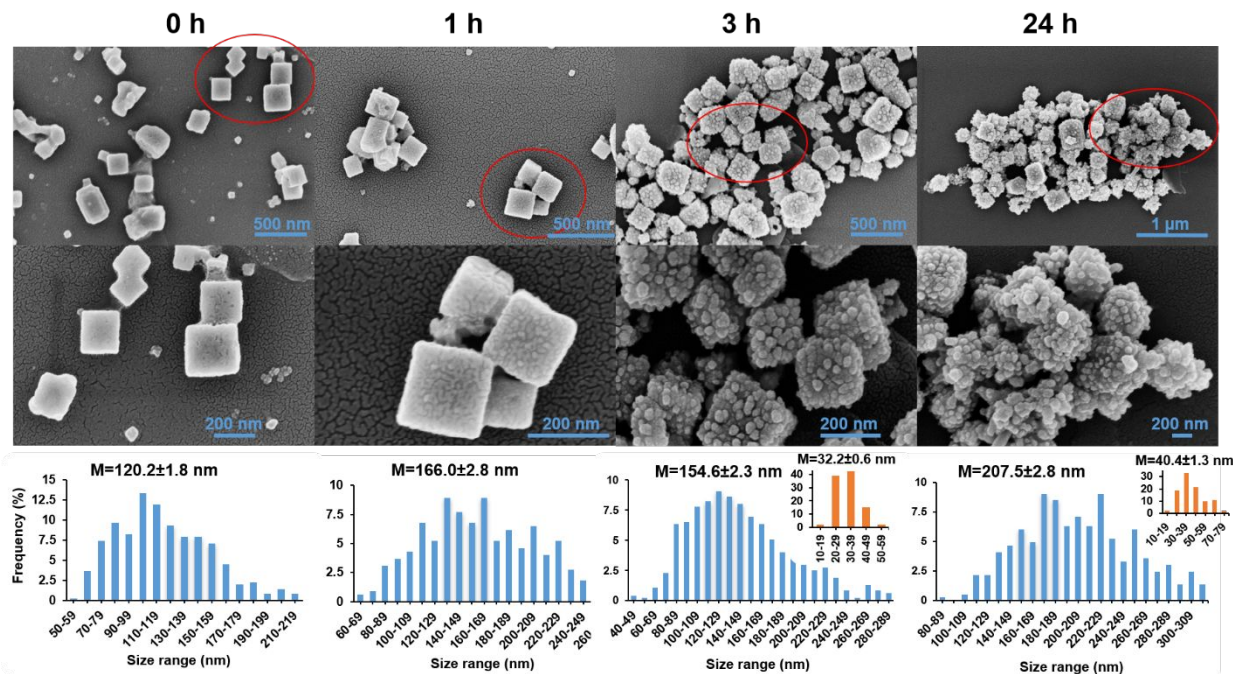


Figure 4. SEM characterization of the morphology and size of the formed particles at different light irradiation intervals (0 h, 1 h, 3 h, and 24 h). The size distribution was based on the length measurements of 338-543 individual particles (small spherical particles formed on the surface of an individual particle were not accounted). The subset panel at 3 h and 24 h shows the size distribution of the small spherical nanoparticles formed on the larger cubic particle surfaces (based on measurements of 130-170 particles). M represents the mean value \pm standard error.

In addition to characterizing the size and morphology of the formed particles over time, we also performed EDS analysis on the formed particles at 0 h (Figure 5a1-a3) and 24 h (Figure 5b1-b3). Two detection modes (points or square areas) were used to compare the surface composition of the cubic microcrystals and spherical nanoparticles. For each mode, 3 replicates were selected. As shown in Figure 5a-b, across all selected points and square areas, Ag emission (Ag $L\alpha 1$ and Ag $L\beta 1$) after normalization to Cl $K\alpha 1$ was higher in the irradiated group (24 h) than in the non-

irradiated group (0 h). The points selected on the formed spherical nanoparticles had the highest Ag emission. These results confirm the transformation of cubic μAgCl to spherical nAg.

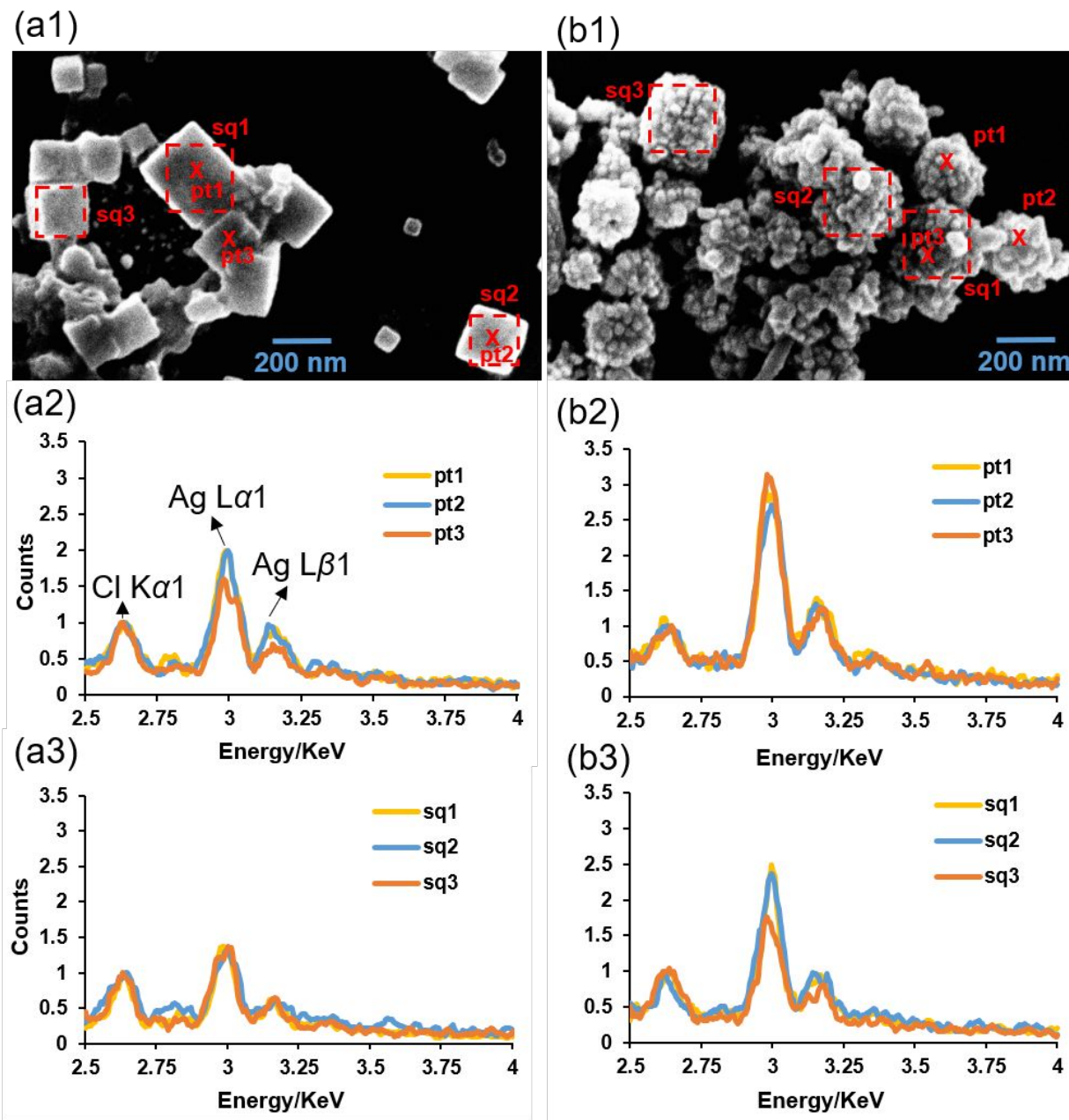


Figure 5. SEM images and corresponding EDS analyses of the particles formed after 0 h (a1-a3) and 24 h (b1-b3) light exposure. Panel a2 and b2 show the EDS results for points (labelled as pt

1
2
3 1-3) while panel a3 and b3 show the EDS analyses for squares (labelled as sq 1-3) after
4
5 normalization to the Cl K α 1 emission.
6
7
8
9

10
11 The formed particles were analyzed by Raman spectroscopy to identify the biomolecules that are
12 associated with the surface and potentially responsible for nAg formation and stability. Raman
13 peak numbers and intensity increased over time (Figure S5), indicating that particles of higher
14 Raman enhancement effect were formed as time elapsed. This is reasonable given the observed
15 gradual changes in size, morphology and composition of the formed particles. As nAg was
16 growing on the μ AgCl surface, the Raman signals of organic ligands attached on the particle
17 surface were enhanced and the surface chemistry pattern became more noticeable. The
18 underlying mechanism is that surface enhanced Raman scattering (SERS) is induced by the
19 formed nAg; the SERS effect is dependent on particle composition, individual particle size, and
20 spatial arrangement.^{48,49} In general, nAg instead of μ AgCl are effective SERS substrate and the
21 effect is greater when the size of individual nAg increases in the range of 0-100 nm²⁹ and when
22 the interparticle distance decreases to <10 nm.⁴⁹ The assignment of the SERS signals of the
23 surface ligands on particles at 24 h are listed in Figure S5.⁵⁰ The Raman peaks observed at 522
24 and 1042 cm⁻¹ were due to C-C=O bending and C-O stretching, respectively. The band cluster at
25 1265 and 1304 cm⁻¹ corresponds to an imidazole ring in-phase breathing mode, a functional
26 group commonly seen in biomolecules such as histidine. The sharp strong peak at 1353 cm⁻¹ is
27 allocated to CH₃ bending or COO⁻ stretching. The three wide strong peaks at 1476, 1568, and
28 2926 cm⁻¹ can be attributed to C-H stretching, COO⁻ stretching or NH₂ deformation, and C-H
29 stretching in -CH₃ and -CH₂-, respectively. The peak assignments specify that the surface ligands
30
31
32
33
34
35
36
37
38
39
40
41
42
43
44
45
46
47
48
49
50
51
52
53
54
55
56
57
58
59
60

1
2
3 of the formed particles may contain amino acids and more complex biomolecules such as
4
5 peptides and proteins.
6

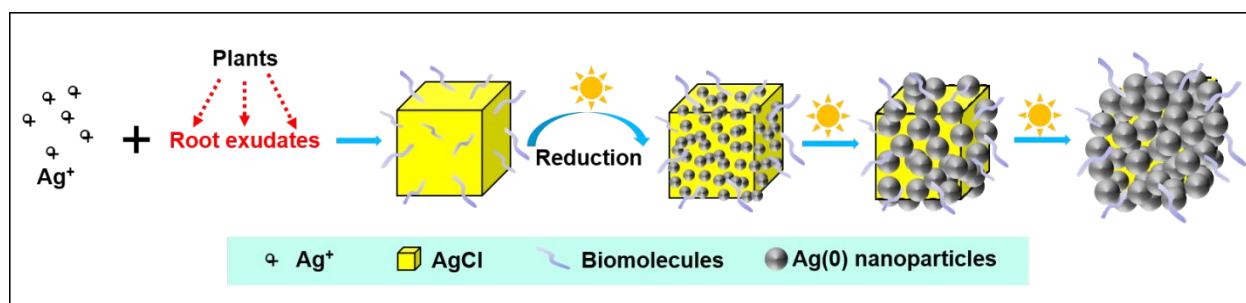
7
8 FTIR analysis was performed to further characterize the biomolecules attached on nAg/ μ AgCl
9
10 surfaces. Across all samples at 0 h or 24 h, five pronounced peaks at 3302, 2928, 1586, 1376,
11
12 1002 cm^{-1} were evident in the range of 650-4000 cm^{-1} (Figure S6). The corresponding
13
14 assignments are O-H stretching, C-H stretching in $-\text{CH}_3$ and $-\text{CH}_2-$, COO^- stretching or NH_2
15
16 deformation, CH_3 deformation or COO^- stretching, and C-O stretching, respectively.⁵⁰
17
18 Interestingly, there is one peak at 1654 cm^{-1} that was absent in 0 h sample but appeared at 24 h;
19
20 this is derived from C=O stretching.⁵⁰ The appearance of this peak may be attributed to the
21
22 photooxidation of biomolecules after long time light exposure, given that light-irradiated μ AgCl
23
24 can generate oxidative holes when electrons were photoexcited from valance band to conduction
25
26 band.^{25,51} The photoirradiation-induced surface chemistry change may be part of the reason why
27
28 nAg/ μ AgCl were unstable and prone to aggregates at 24 h. Combining FTIR spectra with Raman
29
30 data, the surface biomolecules on nAg/ μ AgCl surface were likely amino acids or their
31
32 assemblies (i.e., peptides or proteins) and potentially responsible for the stability of the formed
33
34 nAg. Similar finding was also reported by a study on nAg formation in Ag^+ -amended exudates of
35
36 protozoa.⁵²
37
38
39
40
41
42

43 **Proposed mechanism**

44
45
46 Given the above findings, we propose the following mechanism for the exogenous
47
48 transformation of Ag^+ in plant root zone: 1) initial formation of μ AgCl through complexation of
49
50 Ag^+ by plant-released Cl^- in root exudates; 2) stabilization of μ AgCl by biomolecules present in
51
52 root exudates; and 3) partial photoreduction of μ AgCl to nAg. A schematic illustration of the
53
54 transformation process is shown in Figure 6. We detected 0.57 ± 0.001 mM of Cl^- in root exudates,
55
56
57
58
59
60

1
2
3 which tended to bind Ag^+ to form μAgCl due to the low solubility product equilibrium constant
4
5 ($K_{\text{sp}}=1.77\times 10^{-10}$). This formed μAgCl then provided a substrate platform for the subsequent
6
7 phototransformation of Ag^+ . Importantly, without Cl^- , direct reduction of free Ag^+ to nAg is not
8
9 thermodynamically feasible given that the redox potential ($\text{Ag}^+ + \text{e}^- \rightleftharpoons \text{Ag}^0$, $E^0 = -1.8 \text{ V}$) is
10
11 negative and Ag^+/e^- are more stable than Ag atoms.^{11,53,54} This is particularly evident when there
12
13 are ligands tightly bound to Ag^+ , such as histidine that contains imidazole ring;^{55,56} the hindrance
14
15 of Ag atom deposition by Ag^+ -binding ligands makes the Ag^+ reduction more difficult.⁵⁷ As
16
17 shown in the Raman data, the particle surface was coated by imidazole-containing biomolecules.
18
19 However, in the root exudates the presence of Cl^- led to the formation of μAgCl and allowed for
20
21 the deposition of Ag atoms. The formation of nAg became exergonic (+0.8 V) and
22
23 thermodynamically feasible on μAgCl surfaces.^{11,53,54} Moreover, the μAgCl is photoreactive and
24
25 can produce electron-hole pairs due to photoexcitation of electrons from the valance band to the
26
27 conduction band.^{25,58} The electron-hole pairs can lead to the reduction of μAgCl to nAg on the
28
29 microcube surface.^{25,51,57,59} As photoirradiation time increased, the nAg grew larger, which
30
31 altered the cubic structure of μAgCl to cauliflower-shaped $\text{nAg}/\mu\text{AgCl}$ with nAg studded on the
32
33 surface of the μAgCl . The continuous growth of the nAg blocked light irradiation and
34
35 subsequently decreased the reduction rate. We also constructed a kinetic model for the
36
37 transformation process (Figure S8), which fits ($R^2=0.99$) a second order reaction ($k=1.11 \text{ mM}^{-1}$
38
39 $\cdot \text{h}^{-1}$) and is in agreement with the predicted reaction equation of $2\text{AgCl} \rightarrow 2\text{Ag}(0) + \text{Cl}_2$. In
40
41 addition to Cl^- , the organic compounds released by plant roots also played an important role in
42
43 this process. As indicated by Raman and FTIR data, the formed $\text{nAg}/\mu\text{AgCl}$ was surface
44
45 stabilized by organic molecules containing a number of functional groups such as COO^- , NH_2 ,
46
47 O-H , C-O , or C-H , which are likely from amino acid-based biomolecules. These biomolecules
48
49
50
51
52
53
54
55
56
57
58
59
60

1
2
3 protect the μAgCl from aggregation by forming a stabilizing organic surface layer. This
4
5 protective layering improved the stability of μAgCl and ensured the formation of nanoscale
6
7 silver particles during the photoreduction process. To demonstrate the stabilizing effect of
8
9 organic compounds in root exudates, a mixture of Ag^+/Cl^- (0.37 mM/0.57 mM) in nanopure
10
11 water was tested as a negative control. Without the presence of organic compounds in root
12
13 exudates, AgCl could still be photoreduced to $\text{Ag}(0)$. However, the formed particles were very
14
15 unstable and vulnerable to precipitation after 6 h (Figure S9). In addition to the stabilizing effect,
16
17 we also examined the reducing function of biomolecules in root exudates, as previous studies
18
19 have shown that organic matter, such as NOM and EPS, can induce nAg formation through Ag^+
20
21 reduction. In order to exclude the interference by the photoreduction of AgCl , we removed Cl^- in
22
23 root exudates using the method described above. No nAg formation was observed with
24
25 biomolecules present but without Cl^- in root exudates (Figure S10), suggesting that the
26
27 transformation of Ag^+ to nAg depended on the photoreduction of AgCl , and organic molecules
28
29 themselves cannot reduce Ag^+ to nAg.
30
31
32
33
34
35



46
47 Figure 6. A schematic illustration of the proposed mechanism for the wheat root exudate-
48
49 mediated transformation of Ag^+ to nAg/ μAgCl under light irradiation. When Ag^+ was released
50
51 into the plant root zone, AgCl microcubes (μAgCl) could be formed through the complexation of
52
53 plant-released chloride ions in root exudates with Ag^+ ; meanwhile, biomolecules in root exudates
54
55 acted as stabilizing agents on the surface of μAgCl . Under light irradiation, μAgCl was partially
56
57
58
59
60

1
2
3 photoreduced to Ag(0) nanoparticles (nAg), which led to the morphological change from cubic
4 AgCl microcrystals to cauliflower-shaped core-shell structures with nAg clusters as the shell and
5 μAgCl as the core.
6
7
8
9

10 In the above studies, we investigated the formation of nAg in the root zone of hydroponically
11 grown wheat plants. To broaden the environmental relevance of this study, we extended our
12 experiments to include an aquatic plant, *Lolium multiflorum*,^{26,27} the roots of which are more
13 commonly grown in aquatic systems with sunlight exposure. Furthermore, we tested if nAg
14 could be formed in plant root zone contaminated by lower concentrations (0.05-0.5 mM) of Ag^+ .
15 From Figure S12, we observed the root exudates from *Lolium multiflorum* could transform Ag^+
16 to nAg over 0-24 h of sunlight irradiation, even at concentrations (0.05-0.5 mM) lower than what
17 we used above. Moreover, the sunlight-induced formation of nAg by the root exudates from
18 *Lolium multiflorum* was also dependent on the photoreduction of AgCl (Figure S12, S13). The
19 simulated scenario can be found in surface waters contaminated by relatively high levels (several
20 mg/L to hundred mg/L) of Ag^+ (e.g., wastewater effluents or mining drainage).^{3,60} In the future,
21 environmental systems with ultralow levels (ng/L- $\mu\text{g/L}$) of Ag^+ should be further investigated.
22 Overall, our findings on hydroponically grown plants provide valuable knowledge on the natural
23 formation of nAg by root exudates from aquatic plants under light exposure. In addition to
24 aquatic environment, the proposed transformation may also occur in terrestrial ecosystem.
25 Although the terrestrial plant root system is mostly covered by soils and has limited light
26 exposure, root exudates are mobile, and very likely to be relocated to the soil surface either by
27 natural forces (e.g., soil water transport/capillary force) or by human activities (e.g., soil tillage
28 and/or irrigation). Under this condition, nAg may still be formed in root exudates due to sunlight
29
30
31
32
33
34
35
36
37
38
39
40
41
42
43
44
45
46
47
48
49
50
51
52
53
54
55
56
57
58
59
60

1
2
3 exposure. Future studies are needed to examine the potential natural generation of nAg in
4
5 terrestrial ecosystem.
6
7

8 **Conclusions**

9

10
11 In this work, we demonstrated the plant root exudates-mediated transformation of Ag^+ to
12
13 nAg/ μAgCl in sunlight-irradiated environment. Through quantifying fractions of Ag^+ , μAgCl
14
15 and nAg at different stages of the transformation and characterizing the morphology and surface
16
17 chemistry of the formed particles, we revealed the mechanism underlying the exogenous
18
19 formation of nAg by live plant roots. Due to the presence of Cl^- and biomolecules, root exudates
20
21 were responsible for initiating the generation of μAgCl and stabilizing the formed particles.
22
23 Moreover, the formation of nAg was triggered by light-driven photoreduction of μAgCl . Our
24
25 results provide new insight into the speciation and transformation mechanism of Ag^+ in the
26
27 presence of root exudates, which is important for accurately determining their impact on
28
29 environmental health and agricultural safety. As little information is available in the literature on
30
31 the bio-induced transformation of Ag^+ to nAg in the plant root zone, our work provides a new
32
33 perspective on the fate and behavior of Ag ions and particles in the environment. For example,
34
35 when studying the toxicity of engineered nAg, most published studies use a control group with
36
37 Ag^+ to demonstrate the difference between ionic and nano counterparts. However, without
38
39 considering the possibility of Ag^+ transformation to μAgCl and nAg under the exposure
40
41 conditions, interpretation of the toxicity differences between the different forms of Ag could be
42
43 confounded. Therefore, a comprehensive understanding of the exogenous transformation of Ag^+
44
45 to nAg/ μAgCl in the plant root zone is crucial for evaluating their bioavailability, tropical
46
47 transfer and environmental safety.
48
49
50
51
52
53
54
55
56
57
58
59
60

1
2
3 Our work is among the first to demonstrate the important role of components in plant root
4 exudates in mediating the formation of nAg/ μ AgCl under light irradiation. Further
5 environmental significance can be achieved by expanding this study to other environmental
6 media, such as soil extracts and natural water bodies, since they not only contain a variety of
7 biomolecules but also different inorganic ligands. In addition to Cl⁻, sulfur ions (S²⁻) and sulfate
8 (SO₄²⁻) are also of interest because of their potential redox cycling in the environment and the
9 high binding ability of S²⁻ to Ag. Especially, recent studies have shown that Ag₂S is not as stable
10 as we expected. It was reported that Ag₂S could be transformed to dissolved Ag(I) complexes
11 and/or AgCl particulates due to the oxidation by ozone and chlorine, which are commonly used
12 for WWTP treatments.⁶¹ Li et al. also showed that Ag₂S could be converted to Ag⁺ and nAg
13 through photo-induced redox cycling of Fe²⁺/Fe³⁺.⁶² Moreover, the transformation from S²⁻ to
14 SO₄²⁻ can be found when S-oxidizing bacteria are present in the environment,^{63,64} which may
15 affect the interaction with Ag species. Therefore, the conversion of Ag₂S to Ag⁺, AgCl or nAg is
16 possible in the natural environment. Given that the transformation between metal ions and
17 particulates can modify their biological impacts on various organisms (*e.g.*, crop plants, bacteria
18 and animals),^{7,12,52} it is important to conduct further investigations on how different natural
19 ligands/media affect the Ag speciation and behavior in the environment.
20
21
22
23
24
25
26
27
28
29
30
31
32
33
34
35
36
37
38
39
40
41
42

43 **Conflicts of interest**

44
45
46
47 There are no conflicts to declare.
48
49

50 **Acknowledgements**

51
52
53
54 The authors acknowledge the financial support by USDA NIFA Hatch Program (MAS00475),
55 USDA-NIFA (2015-67017-23070), and BARD (IS-4964-16R) for this work.
56
57
58
59
60

References

- 1 S. Chernousova and M. Epple, *Angew. Chemie - Int. Ed.*, 2013, **52**, 1636–1653.
- 2 A. B. G. Lansdown, in *Current Problems in Dermatology*, 2006, vol. 33, pp. 17–34.
- 3 S. W. P. Wijnhoven, W. J. G. M. Peijnenburg, C. a Herbets, W. I. Hagens, A. G. Oomen, E. H. W. Heugens, B. Roszek, J. Bisschops, I. Gosens, D. Van De Meent, S. Dekkers, W. H. De Jong, M. van Zijverden, A. J. a M. Sips and R. E. Geertsma, *Nanotoxicology*, 2009, **3**, 109–138.
- 4 A. Gogos, K. Knauer and T. D. Bucheli, *J. Agric. Food Chem.*, 2012, **60**, 9781–9792.
- 5 Z. M. Xiu, J. Ma and P. J. J. Alvarez, *Environ. Sci. Technol.*, 2011, **45**, 9003–9008.
- 6 Z. Xiu, Q. Zhang, H. L. Puppala, V. L. Colvin and P. J. J. Alvarez, *Nano Lett.*, 2012, **12**, 4271–4275.
- 7 C. Levard, E. M. Hotze, G. V. Lowry and G. E. Brown, *Environ. Sci. Technol.*, 2012, **46**, 6900–6914.
- 8 W. Hou, B. Stuart, R. Howes and R. G. Zepp, *Environ. Sci. Technol.*, 2013, **47**, 7713–7721.
- 9 Y. Yin, J. Liu and G. Jiang, *ACS Nano*, 2012, **6**, 7910–7919.
- 10 Y. Yin, M. Shen, X. Zhou, S. Yu, J. Chao, J. Liu and G. Jiang, *Environ. Sci. Technol.*, 2014, **48**, 9366–9373.
- 11 N. F. Adegboyega, V. K. Sharma, K. M. Siskova, R. Vecerova, M. Kolar, R. Zbořil and J. L. Gardea-Torresdey, *Environ. Sci. Technol.*, 2014, **48**, 3228–3235.
- 12 F. Kang, P. J. Alvarez and D. Zhu, *Environ. Sci. Technol.*, 2014, **48**, 316–322.
- 13 F. Kang, X. Qu, P. J. J. Alvarez and D. Zhu, *Environ. Sci. Technol.*, 2017, **51**, 2776–2785.
- 14 J. L. Gardea-Torresdey, E. Gomez, J. R. Peralta-Videa, J. G. Parsons, H. Troiani and M. Jose-Yacaman, *Langmuir*, 2003, **19**, 1357–1361.

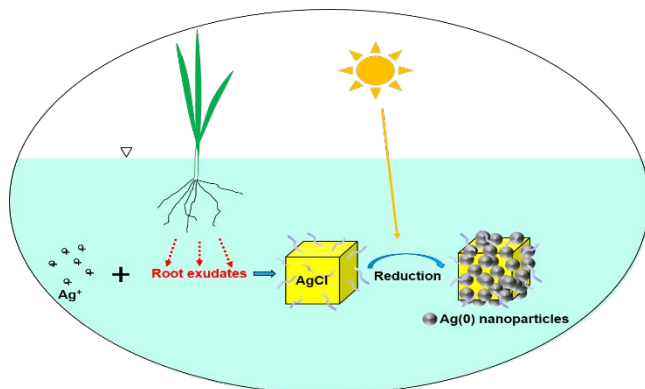
- 1
2
3 15 P. Pardha-Saradhi, G. Yamal, T. Peddisetty, P. Sharmila, S. Nagar, J. Singh, R. Nagarajan and K.
4 S. Rao, *PLoS One*, 2014, **9**, 1–13.
5
6
7
8 16 P. Singh, Y. J. Kim, C. Wang, R. Mathiyalagan and D. C. Yang, *Artif. Cells, Nanomedicine,*
9 *Biotechnol.*, 2016, **44**, 1150–1157.
10
11
12 17 S. Poopathi, L. J. De Britto, V. L. Praba, C. Mani and M. Praveen, *Environ. Sci. Pollut. Res.*, 2015,
13 **22**, 2956–2963.
14
15
16
17 18 R. Amooaghaie, M. R. Saeri and M. Azizi, *Ecotoxicol. Environ. Saf.*, 2015, **120**, 400–408.
18
19
20 19 N. Shabnam, P. Sharmila, Govindjee, H. Kim and P. Pardha-Saradhi, *Front. Plant Sci.*, 2017, **8**, 1–
21 14.
22
23
24 20 N. Shabnam, P. Sharmila, H. Kim and P. Pardha-Saradhi, *PLoS One*, 2016, **11**, 1–13.
25
26
27 21 X. Yang, A. P. Gondikas, S. M. Marinakos, M. Auffan, J. Liu, H. Hsu-Kim and J. N. Meyer,
28 *Environ. Sci. Technol.*, 2012, **46**, 1119–1127.
29
30
31
32 22 C. Levard, S. Mitra, T. Yang, A. D. Jew, A. R. Badireddy, G. V. Lowry and G. E. Brown, *Environ.*
33 *Sci. Technol.*, 2013, **47**, 5738–5745.
34
35
36
37 23 Z. Shen, B. Liu, V. Pareek, S. Wang, X. Li, L. Liu and S. Liu, *RSC Adv.*, 2015, **5**, 80488–80495.
38
39
40 24 G. Wang, T. Nishio, M. Sato, A. Ishikawa and K. Nambara, *Chem. Commun.*, 2011, **47**, 9426–
41 9428.
42
43
44 25 S. Garg, H. Rong, C. J. Miller and T. D. Waite, *J. Phys. Chem. C*, 2016, **120**, 5988–5996.
45
46
47 26 L. Yin, B. P. Colman, B. M. McGill, J. P. Wright and E. S. Bernhardt, *PLoS One*, 2012, **7**, e47674.
48
49
50 27 X. Zhou, G. Wang and F. Yang, *Desalination*, 2011, **273**, 366–374.
51
52 28 T. Yamauchi, K. Watanabe, A. Fukazawa, H. Mori, F. Abe, K. Kawaguchi, A. Oyanagi and M.
53 Nakazono, *J. Exp. Bot.*, 2014, **65**, 261–273.
54
55
56
57
58
59
60

- 1
2
3 29 H. Guo, Z. Zhang, B. Xing, A. Mukherjee, C. Musante, J. C. White and L. He, *Environ. Sci.*
4 *Technol.*, 2015, **49**, 4317–4324.
5
6
7
8 30 Y. Yin, W. Xu, Z. Tan, Y. Li, W. Wang, X. Guo, S. Yu, J. Liu and G. Jiang, *Environ. Pollut.*,
9 2017, **220**, 955–962.
10
11
12 31 W. Hou, B. Stuart and R. G. Zepp, *Environ. Sci. Technol.*, 2013, **47**, 7713–7721.
13
14
15 32 S. Kracht, M. Messerer, M. Lang, S. Eckhardt, M. Lauz, B. Grobéty, K. M. Fromm and B. Giese,
16 *Angew. Chemie - Int. Ed.*, 2015, **54**, 2912–2916.
17
18
19
20 33 M. Darroudi, M. Bin Ahmad, A. H. Abdullah and N. A. Ibrahim, *Int. J. Nanomedicine*, 2011, **6**,
21 569–574.
22
23
24 34 V. K. Sharma, R. A. Yngard and Y. Lin, *Adv. Colloid Interface Sci.*, 2009, **145**, 83–96.
25
26
27 35 O. Zuas, N. Hamim and Y. Sampora, *Mater. Lett.*, 2014, **123**, 156–159.
28
29
30 36 K. Anandalakshmi, J. Venugobal and V. Ramasamy, *Appl. Nanosci.*, 2016, **6**, 399–408.
31
32
33 37 K. I. Peterson, M. E. Lipnick, L. A. Mejia and D. P. Pullman, *J. Phys. Chem. C*, 2016, **120**,
34 23268–23275.
35
36
37 38 M. Sharma, B. Das, J. C. Sarmah, A. Hazarika, B. K. Deka, Y. Park and K. K. Bania, *J. Mater.*
38 *Chem. A Mater. energy Sustain.*, 2017, **00**, 1–11.
39
40
41
42 39 B. A. Rasulov, K. D. Davranov and L. Wen, *Microbiology*, 2017, **86**, 182–187.
43
44
45 40 H. Alishah, S. Pourseyedi, S. E. Mahani and S. Y. Ebrahimipour, *RSC Adv.*, 2016, **6**, 73197–
46 73202.
47
48
49 41 V. A. Kumar, T. Uchida, T. Mizuki, Y. Nakajima, Y. Katsube, T. Hanajiri and T. Maekawa, *Adv.*
50 *Nat. Sci. Nanosci. Nanotechnol.*, 2016, **7**, 015002.
51
52
53
54 42 H. Guo, B. Xing and L. He, *Environ. Pollut.*, 2016, **211**, 198–205.
55
56
57
58
59
60

- 1
2
3 43 H. Guo, B. Xing, L. C. Hamlet, A. Chica and L. He, *Sci. Total Environ.*, 2016, **554–555**, 246–252.
4
5
6 44 B. Andryushechkin, K. Eltsov and V. Shevlyuga, *Surf. Sci.*, 1999, **435**, 109–113.
7
8 45 J. Liu, D. A. Sonshine, S. Shervani and R. H. Hurt, *ACS Nano*, 2010, **4**, 6903–6913.
9
10
11 46 I. Piwoński, K. Spilarewicz-Stanek, A. Kisielewska, K. Kadziola, M. Cichomski and J. Ginter,
12
13 *Appl. Surf. Sci.*, 2016, **373**, 38–44.
14
15
16 47 R. Anderson, R. Buscall, R. Eldridge, P. Mulvaney and P. J. Scales, *Colloids Surfaces A*
17
18 *Physicochem. Eng. Asp.*, 2014, **459**, 58–64.
19
20
21 48 R. A. Halvorson and P. J. Vikesland, *Environ. Sci. Technol.*, 2010, **44**, 7749–7755.
22
23
24 49 H. Guo, L. He and B. Xing, *Environ. Sci. Nano*, 2017, **4**, 2093–2107.
25
26 50 P. J. Larkin, *IR and Raman Spectroscopy - Principles and Spectral Interpretation*, Elsevier, 1st
27
28 edn., 2011.
29
30
31 51 Z. Shen, B. Liu, V. Pareek, S. Wang, X. Li, L. Liu and S. Liu, *RSC Adv.*, 2015, **5**, 80488–80495.
32
33 52 K. Juganson, M. Mortimer, A. Ivask, K. Kasemets and A. Kahru, *Environ. Sci. Process. Impacts*,
34
35 2013, **15**, 244–250.
36
37
38 53 N. F. Adegboyega, V. K. Sharma, K. Siskova, R. Zbořil, M. Sohn, B. J. Schultz and S. Banerjee,
39
40 *Environ. Sci. Technol.*, 2013, **47**, 757–764.
41
42
43 54 S. T. Gentry, S. J. Fredericks and R. Krchnavek, *Langmuir*, 2009, **25**, 2613–2621.
44
45 55 S. Silver, *FEMS Microbiol. Rev.*, 2003, **27**, 341–353.
46
47
48 56 S. Eckhardt, P. S. Brunetto, J. Gagnon, M. Priebe, B. Giese and K. M. Fromm, *Chem. Rev.*, 2013,
49
50 **113**, 4708–4754.
51
52
53 57 V. K. Sharma, J. Filip, R. Zboril and R. S. Varma, *Chem. Soc. Rev.*, 2015, **44**, 8410–8423.
54
55 58 P. Wang, B. Huang, X. Qin, X. Zhang, Y. Dai, J. Wei and M. H. Whangbo, *Angew. Chemie - Int.*
56
57
58
59
60

- 1
2
3 *Ed.*, 2008, **47**, 7931–7933.
4
5
6 59 G. Wang, T. Nishio, M. Sato, A. Ishikawa, K. Nambara, K. Nagakawa, Y. Matsuo, K. Niikura and
7
8 K. Ijro, *Chem. Commun.*, 2011, **47**, 9426–9428.
9
10
11 60 T. W. Purcell and J. J. Peters, *Environ. Toxicol. Chem.*, 1998, **17**, 539–546.
12
13 61 H. Rong, S. Garg and T. D. Waite, *Environ. Sci. Technol.*, 2018, **52**, 11621–11631.
14
15
16 62 L. Li, Q. Zhou, F. Geng, Y. Wang and G. Jiang, *Environ. Sci. Technol.*, 2016, **50**, 13342–13350.
17
18
19 63 F. F. Xia, Y. Su, X. M. Wei, Y. H. He, Z. C. Wu, A. Ghulam and R. He, *Lett. Appl. Microbiol.*,
20
21 2014, **59**, 26–34.
22
23 64 Y. Zhang, X. Wang, Y. Zhen, T. Mi, H. He, Z. Yu and J. Bailey, *Front. Microbiol.*, 2017, **8**, 1–17.
24
25
26
27
28
29
30
31
32
33
34
35
36
37
38
39
40
41
42
43
44
45
46
47
48
49
50
51
52
53
54
55
56
57
58
59
60

Graphical abstract



Silver ions can be naturally transformed to silver nanoparticles due to the plant root exudate-mediated photoreduction of silver chloride microcubes.